iScience

CellPress
OPEN ACCESS

Article

Origin, heterogeneity, and interconversion of noncanonical bistable switches from the positive feedback loops under dual signaling

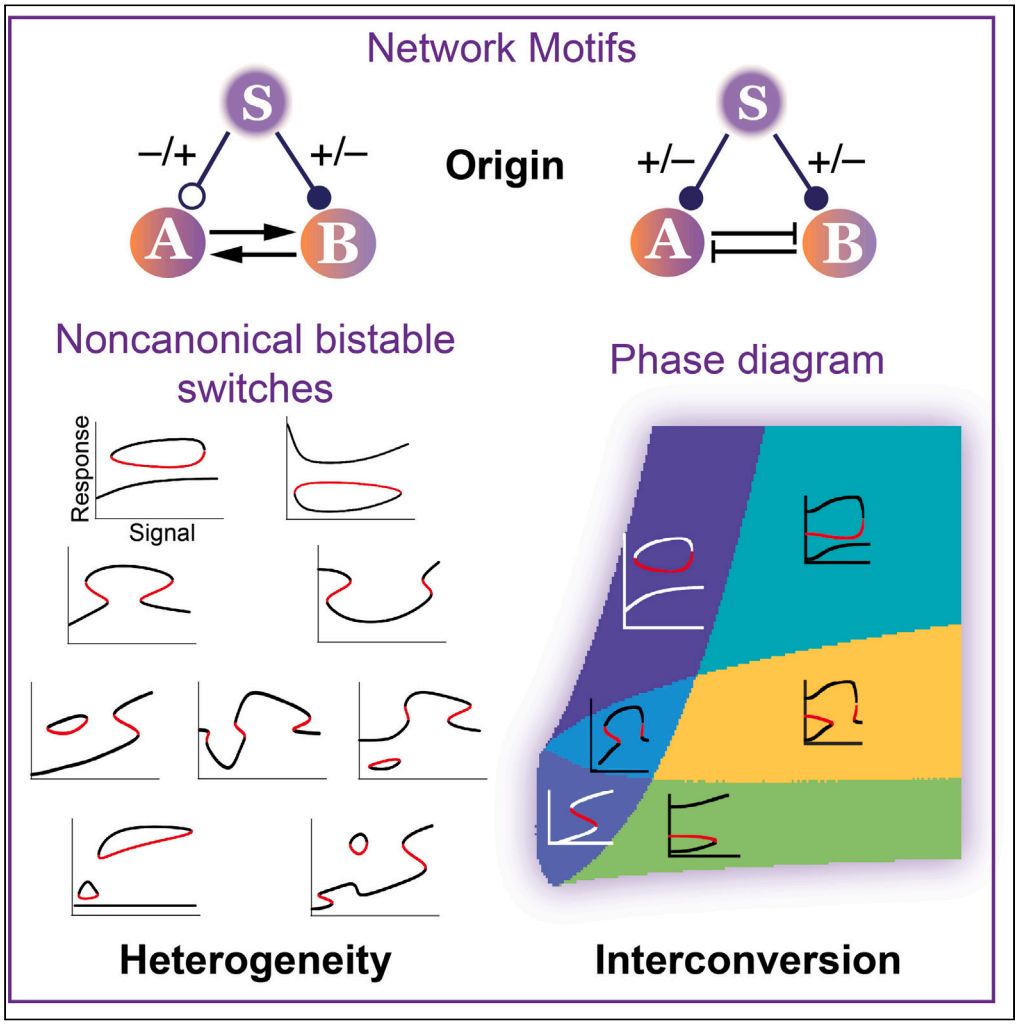

Soutrick Das, Debashis Barik

dbariksc@uohyd.ac.in

Highlights

A single positive feedback loop (PFL) produces a variety of noncanonical bistable switches

Dual signaling is needed for these switches containing one or more bistable regions

Network topological conditions are uncovered from high-throughput bifurcations

Phase diagrams elucidate the mechanism of interchangeability of these switches

Das & Barik, iScience 26, 106379
April 21, 2023
https://doi.org/10.1016/j.isci.2023.106379

iScience

CellPress
OPEN ACCESS

Article

Origin, heterogeneity, and interconversion of noncanonical bistable switches from the positive feedback loops under dual signaling

Soutrick Das[1] and Debashis Barik[1,2,*]

SUMMARY

Designing new functional motifs with unique properties is an important objective in the realm of synthetic biology. We uncover emergent properties of positive feedback loops (PFLs) under dual input signaling using pseudo potential energy-based high-throughput bifurcation analysis. We show that under dual signaling a single PFL generates a variety of noncanonical bistable switches, with one or more bistable regions, due to fusion of multiple canonical bistable switches. Regulatory signs of the dual signaling must be coherent for mutual inhibition loop and incoherent for mutual activation loop of the PFL. Occurrence probabilities show that some of the noncanonical switches, such as isola and mushroom, are highly recurrent under random parameterization. Phase diagrams of the noncanonical switches reveal that feedback strengths of the PFL control the transition from one switch to another. Our calculations decipher the design principles of noncanonical bistable switches that originate from synthetically feasible simple PFL motifs under dual signaling.

INTRODUCTION

Cellular physiological processes are regulated by complex networks of chemical reactions involving diverse types of biomolecules. Complexity of the regulatory networks poses a great difficulty in their characterization and understanding which are crucial in disease context.[1,2] Often many complex networks consist of a core regulatory unit that functions as the main regulatory engine of the physiological processes in the cell.[3] The core regulatory unit can be sliced into functional motifs possessing unique steady state and dynamical properties and thus functional motifs are highly relevant in understanding the behavior of the whole regulatory network. Signal transducer, positive feedback loop (PFL), negative feedback loop, feedforward loop, and antithetic integral feedback loop are some of the important functional motifs that have characteristic properties dictating the behavior of the regulatory network.[4,5] Therefore, discovery of nontrivial properties of functional motifs is an important objective of the current era.

PFL is well-known for its ability to generate bistable signal response curve or bistable switch. Binary decision making processes in living cells are often governed by bistable switch characterized by initial condition dependent gene expression with distinct signaling thresholds of ON and OFF states of the gene.[6] In physiological context bistability has been found to be the principal architect in regulating restriction point in the cell division cycle of mammalian cells,[7–9] entry and exit from mitosis in *Xenopus laevis*,[10,11] programmed cell death by apoptosis,[12–14] mutually exclusive cell fate choices,[15–22] and cellular memory.[23,24] Further genetic engineering technologies lead to the discovery of synthetic toggle switches to regulate metabolism and phenotype with potential applications in engineered cell therapies of human diseases and health.[25–31] Synthetic bistable circuits have also been explored in generating cellular memory which in turn was used to control cellular fates.[32,33] Furthermore, synthetic multistability beyond bistability has recently been stably integrated into mammalian cells with a goal of controlling irreversible cellular fate.[34,35] In a canonical bistable signal response curve, the gene expression changes from low-to-high or high-to-low through a bistable switch and a simple signal transduction of one of the genes in the PFL is sufficient to generate canonical bistable (Bs) switch.[25,36] It creates a dual signaling PFL motif when both the genes in the PFL, created either by mutual inhibition (MI) or mutual activation (MA) loop, are signaled by the same external regulator (Figure 1A). Intuitively such a network motif is expected to generate bistability. However, due to the combinatorial possibilities on the nature of dual input signals, emergent bistable switches may originate as

[1]School of Chemistry, University of Hyderabad, Central University P.O., Hyderabad, Telangana 500046, India

[2]Lead contact

*Correspondence: dbariksc@uohyd.ac.in

https://doi.org/10.1016/j.isci.2023.106379

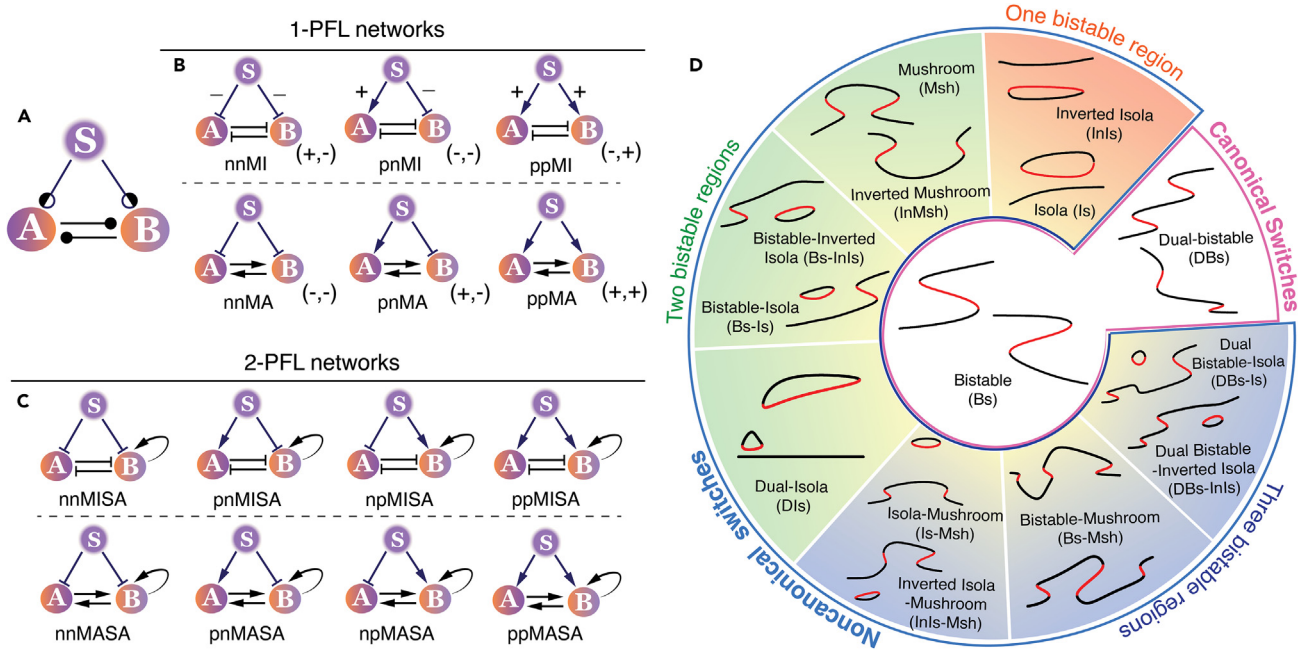

Figure 1. Dual signaling PFL networks and noncanonical bistable switches

The core topology of the dual signaling PFL motif consists of a regulator (S) that signals two genes (A and B) connected by a PFL (A). Arrows with partially filled circles indicate either coherent or incoherent nature of the input signals. A set of three unique networks exist both for the MI and MA loops (B). The arrow- and blunt-headed lines represent activation and inhibition, respectively. In each set, the signs of the input signal are (-,-), (+,-), and (+,+). Beside each network, the signs of the resultant regulation on B via the indirect and direct arms, (+,-) (-,-) and (-,+), are presented. "n" and "p" in the network names represent inhibitory (negative) and activatory (positive) signals on the target genes, respectively. The network becomes asymmetric with the inclusion of a self-activation and a set of four networks possible both for the MISA and MASA motifs (C). The networks are categorized into 1-PFL and 2-PFL motifs based on the number of PFLs in the networks. Bistable switches are categorized into canonical and noncanonical groups and the noncanonical switches are segregated based on the number of bistable regions (D). The switches are represented by the one-parameter bifurcation diagram where the steady state of B is plotted as a function of the signal S. The black and red lines represent the stable and unstable steady states. The complete bifurcation diagrams of these switches are presented in Table S1.

nontrivial properties of the dual signaling PFL motif (Figure 1D). Previous studies have shown that incoherent feedforward signaling of a self-activating gene may result mushroom and isola bistable switches.[37] Mushroom bistability consists of two bistable switches fused in a face-to-face manner with an intervening monostable region. Isola switch, on the contrary, exhibits a single bistable region however with a curious feature of an island of steady states created by a stable and unstable branch.[37,38] In both the switches the expression of the gene changes from low-to-high-to-low (or high-to-low-to-high) as opposed to a canonical switch that exhibits low-to-high (or high-to-low). Mushroom and isola bistable switches have been proposed to govern lineage segregation of neuronal stem cell into either glial cell or neuronal cell under the bone morphogenesis protein 2 (BMP2) signaling.[39] The dual bistable (DBs) switch is another bistable switch, consisting of two bistable regions with intervening monostable region, that exhibits an expression pattern of low-to-intermediate-to-high and originates from the fusion of two canonical bistable switches in a face-to-back manner. DBs switch has been shown to be a key mechanism in the epithelial to mesenchymal transition[21,22] and in tissue homeostasis by Hippo signaling pathway involving Yes-associated protein (YAP) and transcriptional coactivator with PDZ-binding motif (TAZ).[40] In addition to these switches, there could be many other possibilities of noncanonical switches that may originate from the fusion of canonical bistable switches in different orientations (Figure 1 and Table S1).

To determine the network topological and parametric requirements of the noncanonical switches from the PFLs under dual signaling, we used our recently developed pseudo-potential energy based high-throughput bifurcation analysis.[37,41] The potential energy-based bifurcation analysis allowed us to search for 12 different noncanonical bistable switches that include isola, mushroom, bistability with isola, bistability with mushroom, and isola with mushroom all containing one or more bistable regions (Figure 1D). By running tens of millions of bifurcation analysis under random variation of parameters, we determined

the topological criteria of generating noncanonical switches by the dual signaling PFL motif and quantified the chance of obtaining a specific noncanonical switch from a particular network. We generated phase diagrams of the noncanonical switches by running one-parameter (1-p) bifurcation analysis for varying combinations of two other parameters to uncover the heterogeneity of bistable switches and the condition of transition from one switch to another. Further two-parameter (2-p) bifurcation analysis supplemented the phase diagrams and also determined the parametric dependence of bistable switches and their interconversion. Using phase plane analysis, we determined the distinct origin of some of the prominent noncanonical switches. We performed statistical analysis of the parameters obtained from the search for noncanonical switches to underscore the parametric requirements of noncanonical switches in the dual signaling arms of the PFL.

RESULTS

Network models of PFLs under dual signaling

Figure 1A represents the basic topology of a PFL under dual signaling where both the genes in the PFL are regulated by a common regulator. A PFL can be generated either by MI or by MA loop between the genes and the regulatory nature of the two signaling arms can be coherent (same) or incoherent (different). Therefore, a set of three networks exists each for the MI and MA loops (Figure 1B). Due to the prevalence of fused PFLs in cellular differentiation pathways and cancer metastasis, we investigated MI self-activation (MISA) and MA self-activation (MASA) motifs by introducing a self-activatory PFL in the MI and MA motifs, respectively (Figure 1C). It is well known that depending upon the number of PFLs, networks can produce conventional Bs and DBs switches consisting of one and two bistable regions, respectively, and we categorized these switches as canonical bistable switches (Figure 1D). We envisaged that these networks may generate emergent noncanonical switches and considered a set of 12 reversible noncanonical switches consisting of one or two or three bistable regions (Figure 1D). The full 1-p bifurcation diagrams of these switches are listed in Table S1 and the corresponding parameters are listed in Tables S5 and S6. Isola (Is) and inverted isola (InIs) are the two noncanonical switches that consist of a single bistable region and these switches contain a disconnected stable branch and an isolated island of steady states created by connecting a stable and an unstable branch via two saddle-node (SN) bifurcation points. Mushroom (Msh), inverted mushroom (InMsh), bistable-isola (Bs-Is), bistable-inverted isola (Bs-InIs), and dual isola (DIs) are the noncanonical switches consisting of two bistable regions and four SN bifurcation points. The noncanonical switches with three bistable regions with six SN points are isola-mushroom (Is-Msh), inverted isola-mushroom (InIs-Msh), bistable-mushroom (Bs-Msh), dual bistable-isola (DBs-Is), and dual bistable-inverted isola (DBs-InIs). All noncanonical switches originate from the fusion of two or more canonical/noncanonical switches in various numbers, orientations, and orders.

We used nonlinear ordinary differential equations to model the networks. The ultrasensitive switch of activation/inhibition was represented by Hill functions. We developed and used pseudo-potential energy based high-throughput bifurcation analysis method to carry our 1- and 2-p bifurcation analysis. The mathematical representation of the network and the details of the bifurcation analysis method are described in the STAR Methods section.

Network topological requirements and heterogeneity of switches

First, we determined the topological requirements for generating the noncanonical switches from the counts of bistable responses. Figure 2A shows the total count (and %) of canonical and noncanonical bistable switches for all networks under OR- and AND-gate. A group of networks generates exclusively only canonical bistability without a single noncanonical response, while another group generates both the canonical and noncanonical responses. Close inspection of the networks reveals that the noncanonical bistable switches are produced only when the input signals are coherent ((+,+) or (-,-)) for the MI loop and incoherent ((+,-) or (-,+)) for the MA loop irrespective of the number of PFLs and logic gates (Figure 2B). An alternative view of the topological requirement is that across all PFL networks the resultant regulatory signs (see Figure 1B) from S to B (or S to A) via indirect and direct regulations must be dissimilar ((+,-) or (-,+)). The networks with the same resultant regulatory signs on any gene are not capable of producing noncanonical switches. The presence of the additional self-activation in the fused PFLs does not influence these conclusions and it only increases the absolute counts of bistable switches. Several additional features also emerge from these total counts. The MA loops are capable of producing a larger number of noncanonical switches as compared to the MI loops in both the logic gates. Between OR- and AND-gate, MI loops under OR-gate are more potent in generating noncanonical responses as compared to the AND-gate. It is quite

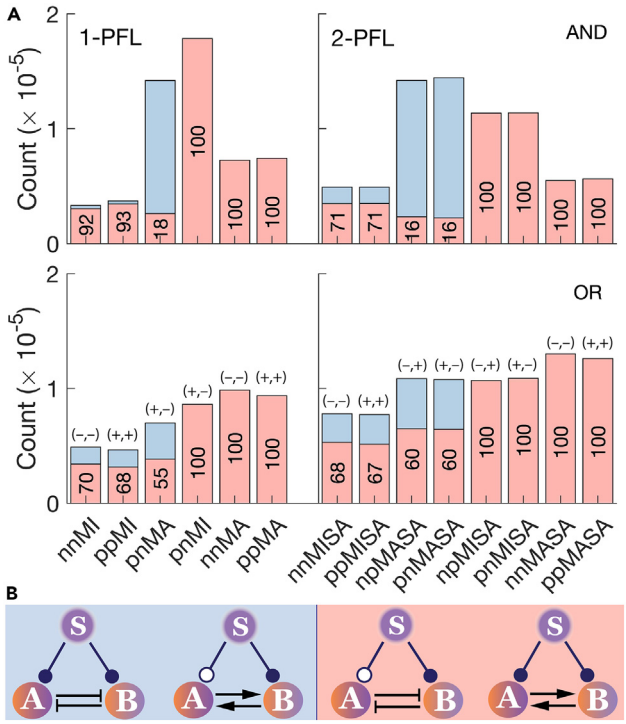

Figure 2. Total counts of canonical and noncanonical switches

The total counts of canonical and noncanonical bistable switches from the networks under OR- (bottom row) and AND-gate (top row) (A). The percentage of canonical switches from a particular network is indicated within each bar. The signs of the two input signaling arms of each network are indicated at the top of the corresponding bar. The MI and MA loops under coherent and incoherent signaling, respectively, are capable of generating noncanonical bistability (B, left). The MI and MA loops do not generate noncanonical switches under incoherent and coherent signaling, respectively (b, right).

remarkable to note that the counts or the percentage of noncanonical responses of a pair of MI networks (nnMI and ppMI or nnMISA and ppMISA) and a pair of MA networks (npMASA and pnMASA) are nearly identical. We verified that the perturbed networks with a single signaling arm do not generate any noncanonical bistability (Figure S1).

We next investigated the heterogeneity of bistable switches from the counts of individual switches from the noncanonical switch-producing networks under OR-gate. The three 1-PFL networks (nnMI, ppMI, and pnMA) produce a large number of canonical Bs switches and do not produce any DBs switch (Figure 3A). On the contrary 2-PFL networks (nnMISA, ppMISA, npMASA, and pnMASA) generate a significant number of DBs. In DBs, the expression level of B changes from low-to-intermediate-to-high (or high-to-intermediate-to-low) and thus requires two-step activation (or inactivation) of the target gene. The additional PFL in the 2-PFL networks allows the two-step activation. For comparison convenience, we segregated noncanonical switches based on the number of bistable regions and compared the counts from all the networks (Figures 3B–3D). Both 1-PFL and 2-PFL networks produce a large number of Is and InIs switches having a single bistable region (Figure 3B). Although 1-PFL MI networks are equally capable of producing both types of isola, however, the 1-PFL MA network produces an overwhelmingly larger number of InIs than the normal Is. Across all 2-PFL networks, InIs is the preferred response as compared to Is. InMsh, Msh, Bs-Is, and Bs-InIs are the switches with two bistable regions and are generated in significant numbers by these networks (Figure 3C). While Msh and InMsh originate from the fusion of two canonical bistable switches, the Bs-Is and Bs-InIs result from the conglomeration of canonical Bs with noncanonical Is (Table S1). Due to their complex nature, the counts of bistability-with-isola switches are significantly less as compared to mushroom switches. Analogous to isola switches, the counts of InMsh are significantly more than the Msh in the 1-PFL MA network and across all 2-PFL networks. It is important to note that, although 1-PFL networks did not generate a single switch consisting of two bistable regions (DBs), however, they generate various noncanonical switches consisting of two bistable regions. The counts of

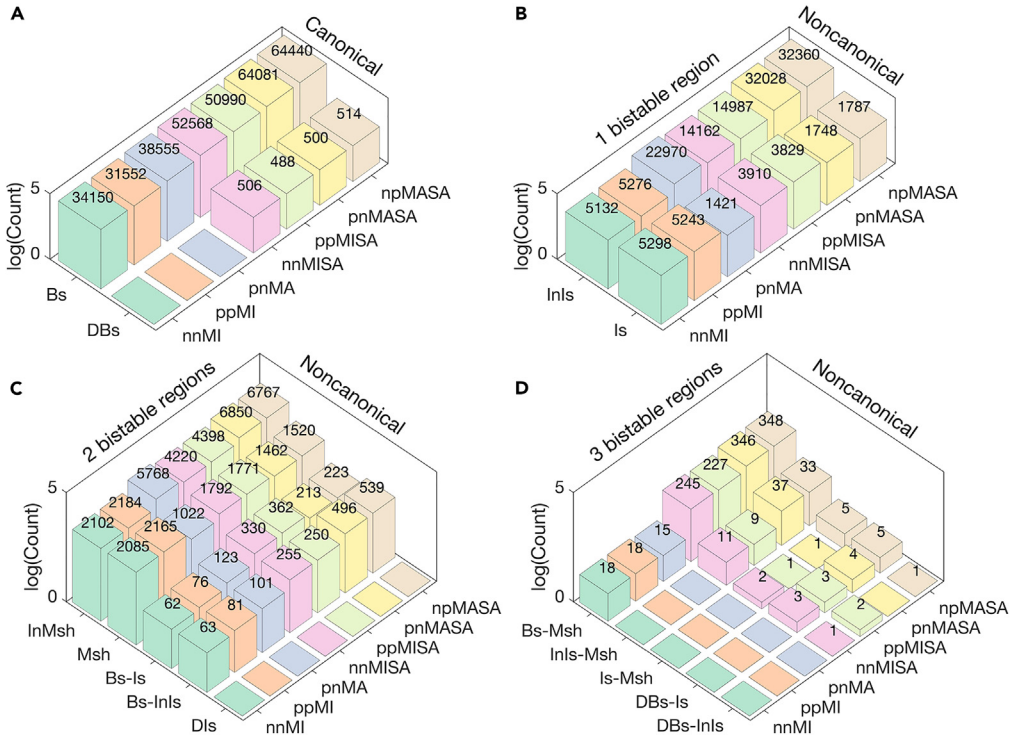

Figure 3. Heterogeneity of canonical and noncanonical switches

The total number of various types of canonical (A) and noncanonical (B–D) bistable switches are presented for the 1-PFL and 2-PFL networks under OR-gate configuration. The noncanonical switches are segregated into one (B), two (C), and three (D) bistable regions.

noncanonical switches with three bistable regions are dramatically less as compared to the two bistable regions (Figure 3D). All five noncanonical switches with three bistable regions originate from the fusion of a canonical/noncanonical switch with another noncanonical switch (Table S1). Bs-Msh is the only noncanonical switch generated by the 1-PFL networks. However, a small number of other switches are also generated by the 2-PFL networks. Therefore, with additional fused PFL the counts of rare switches are expected to increase. In the AND-gate we obtained similar results, however, with shuttle differences. Overall, the heterogeneity of the noncanonical switches is less under AND-gate (Figure S2). As opposed to OR-gate, here the Is and Msh are more than their inverted counterparts. It is also intriguing to note that networks with MA loop here do not generate any inverted switches (InIs or InMsh).

Probability of noncanonical switches

To obtain a quantitative estimation of the probability of obtaining these noncanonical switches, we calculated the percentage chance (% Chance) of noncanonical switches by normalizing their counts with the total count of all bistable switches (Figures 4A and 4B). The % Chance shows that the likelihood of obtaining some of the noncanonical switches is quite high from the dual signaling PFL networks. Among all the noncanonical switches, InIs is the most likely outcome both from the MI and MA networks. In fact, there is one in three chances of obtaining an InIs in MA networks. InMsh is the second most probable noncanonical switch in MA networks. The chances of generating isola and mushroom are significant in MI networks. The probability of obtaining more complex switches involving three bistable regions is relatively less from networks with a single PFL. However, the counts 2-PFLs indicate that complex switches are possible in fused PFL networks. The % Chance of noncanonical switches from the MI networks having (+,+) input signals correlates very well with that of the networks having (-,-) input signals (ppMISA vs. nnMISA and ppMI vs. nnMI) (Figure 4C). Similarly, the MA network with (+,-) input signals shows a good correlation of % Chance with the MA network having (-,+) input signals (Figure 4D). The near perfect correlations suggest that the probability of noncanonical switch does not depend on the specific nature of the input signal pair provided the conditions of dual signaling are satisfied by the network. The % Chance for the AND-gate networks highlights

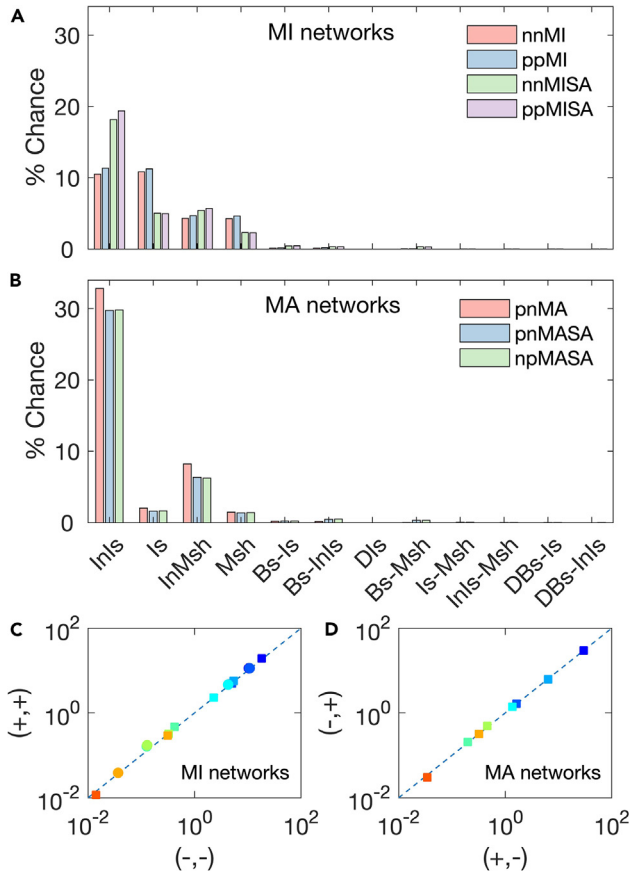

Figure 4. Occurrence probability of noncanonical switches

Comparison of % Chance of obtaining various types of noncanonical switches from the MI and MA networks under OR-gate configuration (A and B). The correlation of % Chance of the noncanonical switches from the MI networks (circle: 1-PFL, square: 2-PFL) under (+,+) input signal with (-,-) input signal (C). Correlation plot for the MA networks with 2-PFLs (D).

the overwhelmingly high probability (~80%) of generating Is switch by the MA network (Figure S3). Further, it also shows that the MA networks under AND-gate are not all capable of producing either InIs or InMsh.

Origin of noncanonical switches: phase-plane analysis.

We next investigated the origin of Is and Msh by analyzing the respective phase-plane diagrams of the dynamical systems of the ppMI network. In Figure 5 we plotted isola bifurcation diagram and its nullclines for different values of S. At small S the two nullclines intersect once leading to a stable steady state with small B. With increase of S, a new intersection of the nullclines occurs at large B leading to the creation of the left SN bifurcation point (point 1) and consequently it generates a stable and an unstable nodes as partners. With further increase of S, the unstable node moves away from the stable partner node and thereby the separation between the stable and the unstable branches increases in the bifurcation diagram. However, with subsequent increase of S, the unstable node starts moving towards the same stable partner node and consequently the gap between the stable and unstable branchs decreases in the bifurcation diagram. Ultimately at large S, these two nodes annihilate each other leading to the second SN point (point 2). Strikingly both the SN points are created by the creation/annihilation of the same set of stable and unstable nodes. Consequently, the resulting stable and unstable branches are connected by two SN points creating an island of steady states in the bifurcation diagram. During this process, the other stable steady node does not undergo any qualitative change and is responsible for creating the disconnected stable branch in the bifurcation diagram. InIs switch also follows similar merging characteristics of the stable and unstable nodes (Figure S4). We emphasize the origin of two SN bifurcation points in the Is switch is completely different from the origin of two SN points in the canonical Bs switch where two different sets of stable and unstable nodes are responsible for generating two SN points (Figure S5).

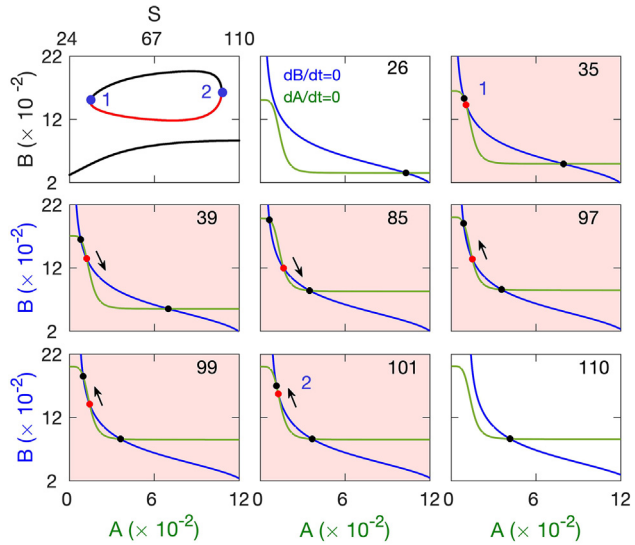

Figure 5. Phase-plane analysis of isola switch

The bifurcation diagram of Is switch and the corresponding phase-plane plots for the indicated values of S for the ppMI network under OR-gate. The two SN bifurcation points are indicated by the blue circles in the bifurcation diagram. The black and red circles at the intersections of two nullclines ($dA/dt = 0$ and $dB/dt = 0$) indicate the stable and unstable nodes, respectively. The parameters for the Is bifurcation are listed in Table S5.

The Msh bifurcation features fusion of two canonical bistable switches in a face-to-face manner with an intervening monostable region (Figure 6). Phase-plane analysis indicates that a pair of new nodes appears after the birth of the first SN point (point 1) and the system becomes bistable. With increasing S the newly born unstable node moves towards the preexisting distant stable node located at low B. The second SN point (point 2) originates from the coalescence of the unstable node with the distant stable node and beyond the second SN point the system becomes monostable with high B. Thus, the forward-facing Bs switch is generated and becomes the left part of the Msh. Subsequent increase of S leads to the birth of the third SN point (point 3) at low B and the system becomes bistable again. The newly born unstable node travels towards the preexisting distant stable node located at high B with progressive increase of S. Finally, the merging of the unstable node with the distant stable node and the annihilation of both of them results in the fourth SN bifurcation point (point 4). The system becomes monostable beyond the fourth SN point and the backward-facing Bs switch is generated as the right part of the MSh. During the entire process, the expression level of B changes from low-to-high-to-low via two different bistable switches and this pattern is different from the DBs switch consisting of two bistable switches where the level of B changes from low-to-intermediate-to-high (Table S1). The behavior of the nullclines for the InMsh is similar to Msh but the expression level of B changes from high-to-low-to-high and two bistable switches congregate in a back-to-back manner in InMsh (Figure S6).

Interconversion of noncanonical switches: phase diagrams

Apart from the topological requirements, parameters are a key factor in determining the response in nonlinear dynamical systems. We envisaged that a particular type of noncanonical switch may transition into another type of switch with the modification of parameters. To determine the condition of interconversion of the various types of switches, we calculated the phase diagrams of the switches by carrying out 1-p bifurcation analysis with respect to S for varying combinations of g_{AB} and g_{BA}—the mutual regulatory strengths of gene A and B on each other. So far, we have considered a total of 14 different bistable switches including two canonical switches. However, considering Bs, Is, and Msh as basic building blocks, various other complex bistable switches may emerge due to the fusion of these three units in different numbers and orientations. We considered a total of 57 different reversible bistable switches consisting up to a maximum of three bistable regions (See Table S7). Furthermore, a bistable switch can be irreversible at the smallest ($S = 0$) or/and at the largest ($S = 1000$) signal values. Irreversibility means the system is bistable at $S = 0$ or/and at $S = 1000$. In order to account for the possibilities of the irreversible switches, an

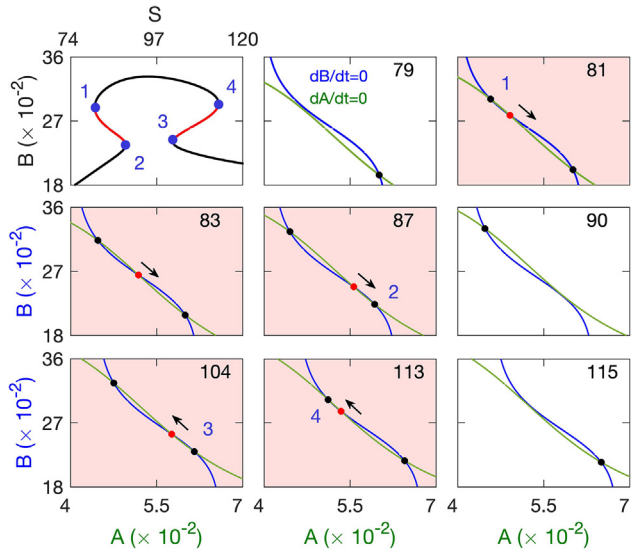

Figure 6. Phase-plane analysis of mushroom switch

The bifurcation diagram of Msh switch and the corresponding nullcline plots for the indicated values of S for the ppMI network under OR-gate. The parameters are listed in Table S5.

additional 69 irreversible switches were considered. Therefore, the phase diagram calculations capable of identifying a bistable switch from a basket of 126 unique bistable switches.

In Figure 7A we plotted the phase diagram of ppMI network starting from Is phase. The Is phase transitions into other bistable phases with the change of feedback strengths represented by the parameters g_{AB} and g_{BA}. The canonical forward facing Bs switch occurs in the region of small g_{AB} and g_{BA}, and this phase changes into a Msh phase with increasing g_{AB}. A backward-facing Bs switch appears along with the existing forward-facing Bs switch to generate Msh switch with increasing g_{AB} (Figure 7B). With further increase of g_{AB}, the Msh phase transforms into an Is phase where the two intermediate SN points of Msh coalesce creating an island of steady states of the Is switch (Figure 7C). Thus, the phase transition between Msh and Is is regulated by the regulatory interaction of gene B on gene A (g_{AB}). On the contrary, with the increase of g_{BA} the Is, Msh, and Bs switches transform into their respective irreversible switches in which the left most SN point lies before $S = 0$ (Figures 7D–7F). The clear phase boundaries between two phases indicate the criticality of the parameter in the transition from one switch to another. Furthermore, the size of the region indicates the robustness of the switches with respect to modification of the parameters. In the ppMISA network with Is as an initial phase, we found a qualitatively similar phase diagram where again g_{AB} dictates the interconversion between Msh and Is (Figure 7G).

The phase diagram calculations determined the effect g_{AB} and g_{BA} on the interconversion of one type of bistable switch to another. We performed next the 2-p bifurcation analysis of the Is switch from the ppMI network with respect to all the synthesis rates in the model (bottom row Figure 7). Conventional 2-p bifurcation analysis determines only the region of bistability by plotting the loci of SN bifurcation points as a function of two parameters. Here in addition to region of bistability, we also determined the identity of the bistable switch during the energy-based bifurcation analysis therefore uncovering the transition of one type of switch to another with the modification of parameters (See STAR Methods for details). The 2-p bifurcation diagram with respect to g_{AB} and g_{BA} are consistent with phase diagrams presented in the Figure 7A. With the increase of g_{AB} the irreversible Bs switch transition into an Is switch with two intervening regions of irreversible Msh and Msh switches. The Is switch transition into an irreversible Is with the increase of g_{BA}. The 2-p bifurcations with respect to basal synthesis rates (g_{A0} and g_{B0}) and regulated synthesis rates by the signal S (g_{AS} and g_{BS}) reveal the robustness of Is switch in terms of the flexibility of parameter variation. Across all parameters Is switch exists adjoining to Msh switch.

We performed phase diagram analysis of InIs switch in ppMI network under OR-gate to uncover that various types of switches exist with the variation of g_{AB} and g_{BA} (Figure 8A). The forward-facing Bs phase

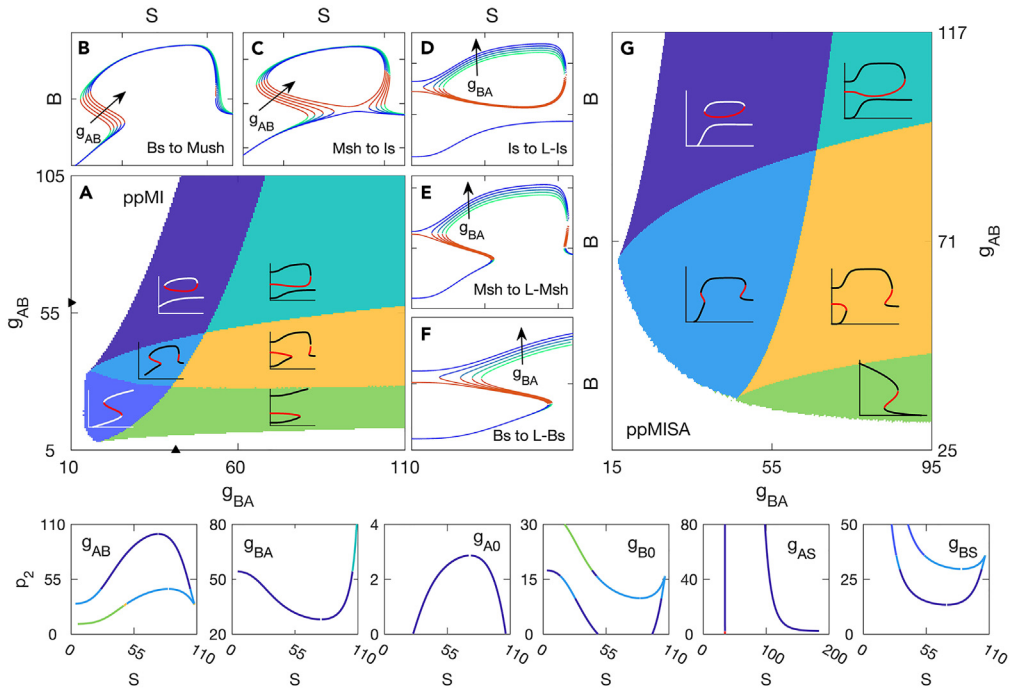

Figure 7. Phase diagrams of initial phase of isola

Phase diagram of Is switch (presented in the Figure 5) as initial phase in ppMI network under OR-gate (A). Bistable phases are indicated by the different colors and the representative 1-p bifurcation plots indicate the phase type (A). The white region represents monostability. 1-p bifurcation plots highlight the transition from Bs to Msh (B), Msh to Is (C), Is to L-Is (D), Msh to L-Msh (E), and Bs to L-Bs (F) with the increasing value of either g_{AB} or g_{BA} (represented by the arrow). The prefix "L" represents irreversibility at the left. Phase diagram of ppMISA network under OR-gate with Is as an initial phase (G). The parameters for the ppMISA phase diagram are listed in Table S8. The plots in the bottom panel represent the 2-p bifurcations of the Is switch from the ppMI network. In the 2-p bifurcation the loci of SN points are plotted as a function S and a secondary parameter as indicated inside each plot. The area enclosed by the curve is bistable and the system is monostable outside. Different colors represent different types of bistable switches and the color scheme is same as in (A). For the 2-p bifurcations with respect to g_{AB} and g_{BA} the corresponding values of g_{BA} and g_{AB}, respectively, are indicated by the triangles in the phase diagram (A).

transitions into InMsh phase with the increase of g_{BA}. With increasing g_{BA}, a new backward-facing Bs switch appears on the left of the existing forward-facing Bs switch creating InMsh (Figure 8B). Subsequently with g_{BA}, the InMsh phase changes into InIs phase where the two intermediate SN points of InMsh converge to produce InIs (Figure 8C). Thus, the transitions between the InMsh and InIs switches are controlled by the regulatory strength of A on B (g_{BA}). These switches transition to their respective irreversible switches on the right with the increase of g_{AB}. The irreversibility on the right is a result of the finite value of the signal ($S = 1000$). At a large g_{AB} the InMsh becomes irreversible on the both sides. We found similar phase transition behavior of the forward facing Bs, InMsh and InIs switches in the case of ppMISA network under OR-gate (Figure 8D). The transition from InIs switch into other types of switches can also be observed in the 2-p bifurcations with respect to g_{AB} and g_{BA} (bottom row, Figure 8) for the ppMI network. Furthermore, the InIs switch is robust to modifications of basal (g_{A0} and g_{B0}) and signal regulated synthesis rates (g_{AS} and g_{BS}) of A and B.

Phase transition calculations starting with mushroom phase in the same network have revealed the existence of diverse types of switches with the variation of g_{AB} and g_{BA} (Figure 9A). Consistent with Is phase diagram, the interchangeability between Is and Msh is controlled by g_{AB}. It is curious to note that with increased g_{BA}, Msh phase changes into Bs-Msh phase consisting of three bistable regions. With increase of g_{BA}, the birth of two new SN points on the stable branch located on the left of the Msh creates a backward-facing Bs and altogether it becomes Bs-Msh (Figure 9B). Subsequent increase of g_{BA} leads to conversion of Bs-Msh into Bs-InIs phase where the inverted mushroom (created by the first two bistable switches) of the Bs-Msh converge to generate the InIs (Figure 9C). Again, the conversion of InMsh into an InIs is

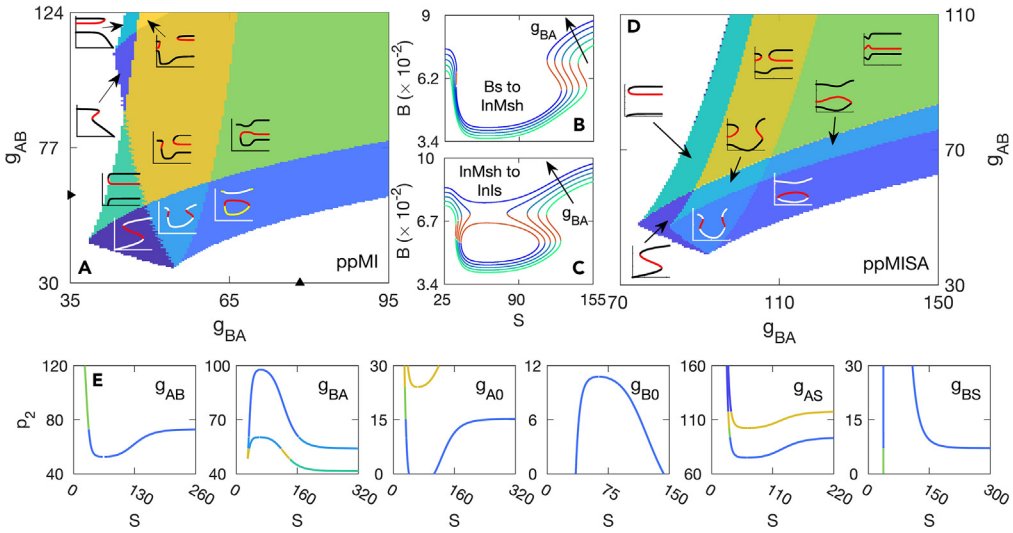

Figure 8. Phase diagrams of initial phase of inverted isola

Phase diagram of ppMI network in OR-gate configuration with InIs as an initial phase (A) (see Table S5 for the parameters). One parameter bifurcation plots show the transition from Bs to InMsh (B) and InMsh to InIs (C) with the variation of g_{BA}. Phase diagram of ppMISA network in OR-gate configuration with InIs as an initial phase (D). The parameters for the ppMISA network with initial InIs phase are listed in Table S8. Bottom row: 2-p bifurcations of the InIs switch from the ppMI network (E). The values of g_{BA} and g_{AB} for the 2-p bifurcations with respect to g_{AB} and g_{BA}, respectively, are indicated by the triangles in the phase diagram in the panel (A). The line colors in the 2-p bifurcations represent different types of bistable switches as represented in the phase diagram of the ppMI network (A).

triggered by g_{BA} as seen in Figure 8. On the contrary, with increase of g_{AB} the Bs-Msh changes into a Bs-Is where the mushroom in the Bs-Msh (last two bistable regions) converges to produce the Is on the right of the first bistable switch (Figure 9D). This transition is again consistent with the findings of Figure 7 where the transition from Msh to Is was found to be regulated by g_{AB}. The existence of Bs-Msh, Bs-InIs and Bs-Is phases underscore that complex switches with multiple bistable regions can be generated by a single PFL under dual signaling. These switches become irreversible on the left at higher values of g_{AB}. In case of InMsh as the initial phase, again we found that the interconversion between InMsh and InIs is dictated by the g_{BA} (Figure 9E). To check the consistency, we performed phase transition calculations of pnMA network with different initial phases and we again found that transition between Is and Msh is regulated by g_{AB} and transition between InIs and InMsh is regulated by g_{BA} (Figure S7 and Table S9).

The 2-p bifurcation analysis of the Msh switch obtained from the ppMI network are presented in the Figure 10. The 2-p bifurcation calculations were performed with respect to all the synthesis rates in the model. These calculations indicate that the Msh switch always remains adjacent to Is switch irrespective of the secondary parameter. 2-p bifurcations with respect to g_{BA} (Figure 10B) shows the complexity of transition from one switch to another. With increase of g_{BA}, the Is with one bistable region transitions into a Msh with two bistable regions. The Msh then becomes Bs-Msh consisting of three bistable regions and it then transitions into a Bs-InIs with two bistable regions. Finally, Bs-InIs changes into a backward-facing Bs switch termed as bistable backward (BsB) consisting of a single bistable region. Similar complexity is also observed in case of g_{B0} where it follows the transition pattern of Is → Msh → Bs-Msh → InMsh → InIs. The 2-p bifurcations with g_{B0} highlights that an Is switch can be converted into an InIs switch with the modification of g_{B0}.

Requirements of dual signaling arms

In addition to the feedback strengths, activation (or inhibition) thresholds are key parameters as they dictate the amount of signal required to flip the state of ultrasensitive switch represented by the Hill function. We investigated the role of signaling thresholds of the two input signaling arms, J_{AS} and J_{BS}, in generating a specific noncanonical response. From the searched parameters for the bistable switches, we calculated the logarithm of the ratio of average J_{AS} and J_{BS} to measure of dissimilarity (or similarity) of the two thresholds. Across all networks and logic gate configurations, the values of these parameters are nearly similar for the canonical Bs switch (Figure 11). However, for the noncanonical switches, the values of these

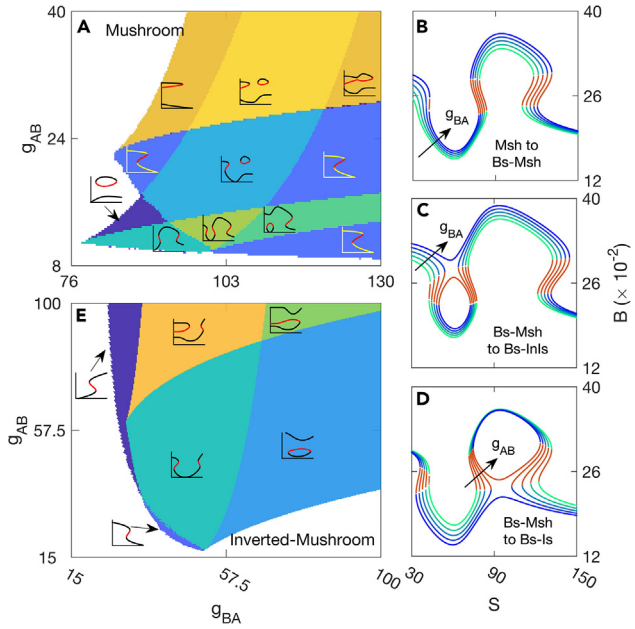

Figure 9. Phase diagrams of initial phase of mushroom

Phase diagrams of ppMI network under OR-gate configuration with Msh (A) and InMsh (E) as initial phases. 1-p bifurcations showcase the transition from Msh to Bs-Msh (B), Bs-Msh to Bs-InIs (C), and Bs-Msh to Bs-Is (D). The parameters for the initial phases are listed in the Table S5.

parameters are dissimilar and follow a pattern based on the type of switch and the network. The ratios indicate that Is and Msh switches require $J_{AS} < J_{BS}$ for the nnMI, nnMISA, pnMA, and pnMASA networks (Figure 11A). A closer inspection reveals that in these four networks the resultant signs of the two arms from S to B is (+,-) (Figure 1B). Both Is and Msh switches exhibit an expression pattern of low-to-high-to-low for B and, therefore, B must be activated first and then deactivated later with signal. In order to satisfy this requirement, the threshold of activation arm (indirect arm; S to B via A) must be smaller than the threshold of deactivation arm (direct arm; S to B) such that B is activated and deactivated at low S and high S, respectively. Consequently, the average J_{AS} was smaller than the average J_{BS} in these four networks. On the contrary, the expression pattern of B in InIs and InMsh is high-to-low-to-high. Therefore, the deactivation and activation of B must occur at the low and high signal, respectively. In order to satisfy this, the threshold of deactivation must be smaller than the threshold of activation and thus these networks show $J_{AS} > J_{BS}$ (Figure 11A). These inequalities become exactly opposite for the ppMI, ppMISA, and npMASA networks whose resultant signs of two signaling arms are (-,+) (Figure 11B). Due to the flipping of the regulatory signs of the signaling arms, the inequalities now become opposite in these networks. The cumulative distributions of the two thresholds also show the consistent dissimilarity patterns for the noncanonical switches (Figure S8). These networks under AND-gate follow similar inequalities (Figures 11C and 11D).

As the relative magnitudes of J_{AS} and J_{BS} are key to obtaining a particular noncanonical switch, we calculated the phase diagrams of Is, Msh, InIs, and InMsh with respect to these two parameters to estimate the phase separation behavior of these switches under the variation of these thresholds (Figure 12). A single phase was obtained in the case of Is, and in case of Msh two other phases were obtained (Figures 12A and 12B). The triangular phase diagrams in these cases indicate the criticality of the ratio of the two activation thresholds. As J_{AS} increases relative to that of J_{BS} the region of Is and Msh phase increases consistent with the inequality conclusion of Figure 11A. On the contrary, as the value of J_{BS} increases relative to J_{AS} the region of InIs and InMsh increases (Figures 12C and 12D). The triangular phase diagrams highlight the importance of relative magnitudes of J_{AS} and J_{BS}.

DISCUSSION

Bistability generated by PFLs has been proven to be a key mechanism in cellular decision making processes and has been investigated extensively. Here we investigated the fate of PFLs under dual signaling where

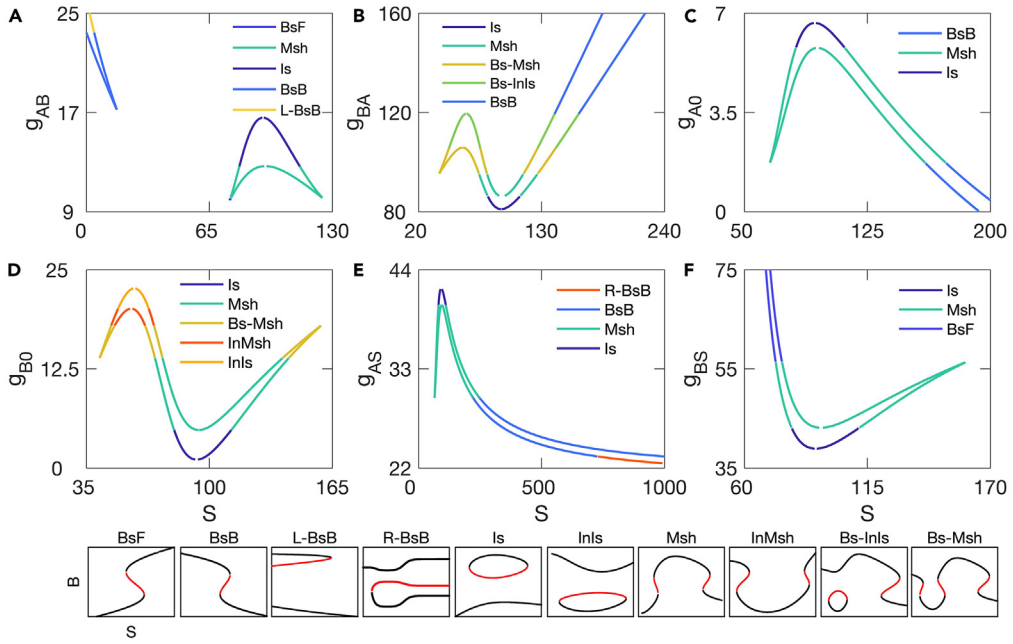

Figure 10. 2-p bifurcation diagrams of MSh

2-p bifurcation diagrams of the Msh switch (in Figure 9A) from the ppMI network (A–F). The regions enclosed by the curves are bistable and outside the system is monostable. Different types of bistable switches are represented by different colors. The color scheme is same as in the phase diagram (Figure 9A). All the different switches observed in the 2-p bifurcation calculations are indicated in the bottom panel for reference.

both the genes in the PFL are regulated by a common regulator. Our objective was to determine the network topological and parametric conditions of generating emergent noncanonical bistable switches that may originate due to fusion of canonical bistable switches in different numbers and orientations, heterogeneity of these switches and the conditions of transitions from one switch type to another type. We developed and used pseudo potential energy based automated high-throughput bifurcation analysis method to search for the emergent noncanonical bistable switches under random parameter variations.

We show that a dual signaling PFL can generate a variety of noncanonical bistable switches consisting of one or multiple bistable regions and these switches become emergent property of the network as removal of one of the input signals does not produce any noncanonical switches. However, dually signaled PFL must satisfy certain topological conditions for producing these emergent switches. To generate noncanonical switches from the MI loops, the two input signaling arms must have same regulatory effects (coherent) on the target genes of the PFL and for the MA loops the regulatory effects must be dissimilar (incoherent) (Figure 2). Results from Figure 2 also establish that the logic gate arrangements of signaling (OR- or AND-gate) and additional PFL in the core networks (2-PFL networks) do not alter the topological requirements of the dual signaling arms. Therefore, topological constraints of dual signaling are generic as they do not depend on the logic gate configurations and the number of additional PFLs in the networks. Heterogeneous types of noncanonical switches consisting of one, two, and three bistable regions are produced only by the networks that satisfy the topological requirements (Figure 3). The extent of heterogeneity depends on the number of fused PFLs in the networks and logic gate configurations. Heterogeneity increases with the number of PFLs and responses from OR-gate networks are more heterogeneous than the AND-gate networks (Figures 3 and S2). In the OR-gate, two input regulations on a target gene function independently and thus flipping the underlying ultrasensitive switch embedded in the PFL occurs in a redundant manner. Consequently, the possibility of generating a noncanonical response increases with random parameter searching leading to heterogeneous noncanonical switches. On the contrary, in the AND-gate configuration, two regulations must be synergistic to flip the ultrasensitive switch. Consequently, the system becomes more restrictive in terms of obtaining a noncanonical response leading to reduction of heterogeneity in types of noncanonical switches.

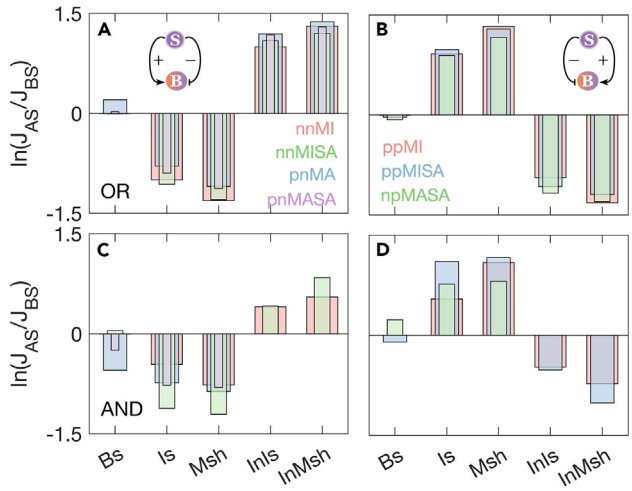

Figure 11. Conditions of threshold parameters

The logarithm of ratio of average J_{AS} and J_{BS} obtained from random parameter search are compared together for the networks whose resultant regulatory signs from S to B are same. In the left (A and C) and right (B and D) panels the resultant signs of the signal from S to B in two arms are (+,-) and (-,+), respectively. These comparisons were made both for the OR- (top panels) and AND-gate (bottom panels) configurations.

The absolute count and occurrence probability show that isola and mushroom switches, both normal and inverted, are highly probable from simple dual signaling PFL motifs (Figure 4). Probability of obtaining more complex switches with more than two bistable regions are generally lower in networks with a single PFL. However, with additional fused PFL, the probability of the complex switches increases, and thus inclusion of multiple PFLs in the minimal motif would increase the possibility of more complex switches. Among the group of noncanonical switches with one, two, and three bistable regions, inverted isola, inverted mushroom, and bistable-mushroom are the most abundant noncanonical switches, respectively. Importantly, the probability of noncanonical switches does not depend on the specific nature of the input signals.

Phase-plane analyses uncover the distinct origin of the isola switches (Figures 5 and 6). The island of steady states in the isola switch originates from the two SN bifurcation points where each SN point is born due to coalescence of the same pair of stable and unstable nodes. On the contrary, in canonical Bs switch a different pair of stable and unstable nodes coalesces for each SN bifurcation point. The unprecedented phase diagram calculations show that diverse types of phases (or switches) with clear phase boundaries are possible and switching from one phase to another is triggered by the modification of mutual regulatory strengths of the two genes (Figures 7, 8, 9, and 10). Across all networks the transitions between the isola and mushroom are controlled by the regulatory strength of the terminal gene on the participating gene in the PFL and transition between the inverted isola and inverted mushroom is dictated by the regulatory strength of the participating gene on the terminal gene. The ratio of signaling thresholds of two input signaling arms are a key factor in determining the types of noncanonical response. Noncanonical switches require distinct values of the two thresholds such that multiple conventional bistable switches can fuse sequentially in opposite orientations to emerge as noncanonical switches (Figures 11 and 12). We emphasize that these conclusions are general due to the random parameter searching approach of the large-scale bifurcation analysis and such analysis was only possible due to the high-throughput bifurcation analysis tool.

Our work is purely synthetic in nature and it predicts the emergent properties of the PFLs under dual signaling. Such a motif is known to exist in several cell fate-choice regulatory networks. In the T helper (T_H) and induced T regulatory (iT_{reg}) cell fate choices, T cell receptor signaling is known to coherently activate the MI loop created by T-bet/RORγ3, T-bet/GATA3, and FoxP3/RORγ3 in the cell fate choice between T_H1/T_H17, T_H1/T_H2, and iT_{reg}/T_H17 cells, respectively.[42–44] TGF-β induced reciprocal cell fates of iT_{reg}/T_H17 cells are regulated by mutual antagonism between FoxP3/RORγ3 where both the transcription factors are coherently activated by TGF- β signaling.[45] The reversible transition from the mesenchymal to amoeboid cell fates in cancer cells is regulated by the network involving a MI loop between the RhoA and Rac1 GTPases and both the GTPases are coherently inhibited by microRNA miR-34 and also separately by

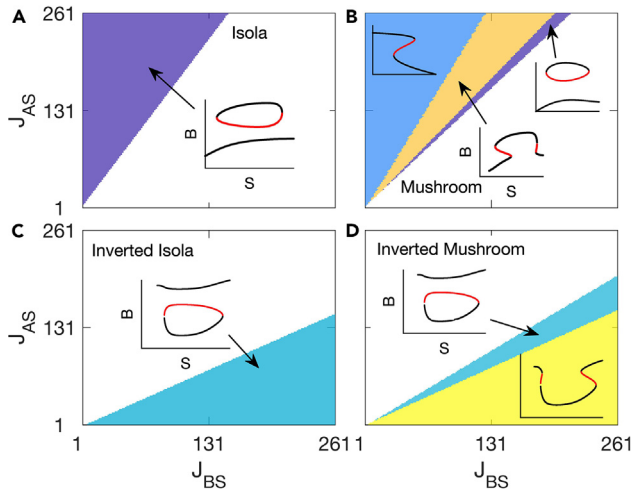

Figure 12. Phase diagrams under threshold parameters

Phase diagrams of Is (A), Msh (B), and InIs (C) and InMsh (D) switches with the variation of the thresholds J_{AS} and J_{BS} for the ppMI network with OR-gate configuration (parameters are listed in Table S5).

miR-200.[46] Due to the less familiarity of the isola and mushroom switches, the relevance of these noncanonical switches have not been explored in these cell fate networks that satisfy the requirements of generating noncanonical switches. However, mathematical modeling previously has uncovered the role of mushroom bifurcation in the fate choice of neuronal stem cell that differentiate into either glial cell or neuronal cell under the BMP2 signaling.[39] A closer inspection of the network reveals the existence of incoherent BMP2 signaling on the expression of self-activating *Mash1* and our calculations also show that MA motif only under incoherent dual signaling can generate mushroom or other noncanonical switches. Altogether, our discovery of emergent switches originating from a simple dual signaling PFL motif has a great potential to be relevant in the cell lineage commitment. Furthermore, the rich behavior of such a simple topology in generating complex switches can also be an area of exploration in the field of synthetic biology. The simplicity of the design principles of network motifs enhances the feasibility of synthetic exploration of unexplored bistable switches experimentally.

The bistable switches in our investigations are generated from networks with explicit PFL with nonlinear kinetics of regulatory interactions. These types of networks are known to present both in gene regulatory and protein interaction networks. However, it is important to note that bistability has also been proven to exist without explicit PFL and nonlinear kinetics through the mechanism of competing multistep phosphorylation/dephosphorylation reaction in mitogen active protein kinase pathway[47] and by molecular titration of mRNA by microRNA in lineage segregation of motor neuron subtypes.[48] Particularly bistability generated from post-transcriptional level interaction between mRNA and microRNA can be a key mechanism for lineage segregation in systems where the gene regulatory network lacks an explicit PFL.

In this work we have only considered bistable switches originating from the SN bifurcations, although bistability can also be due to pitchfork bifurcation.[49] Some of the 1-PFL networks satisfy the symmetry requirement of the network required for pitchfork bifurcation. However, due to the random parameter sampling protocol of our method the parameters become asymmetric diminishing the possibility of pitchfork bifurcation. Previous modeling works on cell fate decision making have shown the relevance of symmetry of parameters in pitchfork bifurcation[42,50–52] and further under broken symmetry a pitchfork bifurcation become an isola switch.[42] In addition, the identification protocol of bistable switches was designed to identify only switches from SN bifurcations ruling out the possibility of percolation of bistable switches from pitchfork bifurcation.

Limitations of the study

The current work uncovers the potential of a single PFL, under dual signaling, in generating diverse types of noncanonical bistable switches that originate from SN bifurcations. However, bistability can be a result of pitchfork bifurcations also. Although pitchfork bifurcations are less common due to the strict symmetry

requirements of the network and parameters, however, the possibility of bistability from such bifurcations can be investigated using potential energy-based bifurcation analysis method.

STAR★METHODS

Detailed methods are provided in the online version of this paper and include the following:

- KEY RESOURCES TABLE
- RESOURCE AVAILABILITY
  - Lead contact
  - Materials availability
  - Data and code availability
- METHOD DETAILS
  - Mathematical models of the networks
  - Bifurcation analysis using pseudo-potential energy
  - Identification of various types of bistable switches
  - Parameter search for bistable switches
  - Phase diagrams of bistable switches
  - 2-p bifurcation analysis
- QUANTIFICATION AND STATISTICAL ANALYSIS
- ADDITIONAL RESOURCES

SUPPLEMENTAL INFORMATION

Supplemental information can be found online at https://doi.org/10.1016/j.isci.2023.106379.

ACKNOWLEDGMENTS

The work was supported by the MATRICS (grant no. MTR/2019/000935) and CRG (grant no. CRG/2019/006999) research grants from the Science and Engineering Research Board, Department of Science and Technology (India) to D.B. S.D acknowledges fellowship from INSPIRE program of Department of Science and Technology, India.

AUTHOR CONTRIBUTIONS

D.B. designed research; D.B. and S.D. performed research, analyzed data and wrote the paper.

DECLARATION OF INTERESTS

The authors declare no competing interests.

INCLUSION AND DIVERSITY

We support inclusive, diverse, and equitable conduct of research.

Received: November 30, 2022
Revised: February 8, 2023
Accepted: March 6, 2023
Published: March 13, 2023

REFERENCES

1. Hanahan, D., and Weinberg, R.A. (2011). Hallmarks of cancer: the next generation. Cell *144*, 646–674. https://doi.org/10.1016/j.cell.2011.02.013.

2. Barabási, A.L., Gulbahce, N., and Loscalzo, J. (2011). Network medicine: a network-based approach to human disease. Nat. Rev. Genet. *12*, 56–68. https://doi.org/10.1038/nrg2918.

3. Alon, U. (2007). Network motifs: theory and experimental approaches. Nat. Rev. Genet. *8*, 450–461. https://doi.org/10.1038/nrg2102.

4. Tyson, J.J., and Novák, B. (2010). Functional motifs in biochemical reaction networks. Annu. Rev. Phys. Chem. *61*, 219–240. https://doi.org/10.1146/annurev.physchem.012809.103457.

5. Khammash, M.H. (2021). Perfect adaptation in biology. Cell Syst. *12*, 509–521. https://doi.org/10.1016/j.cels.2021.05.020.

6. Ferrell, J.E., Jr. (2002). Self-perpetuating states in signal transduction: positive feedback, double-negative feedback and bistability. Curr. Opin. Cell Biol. *14*, 140–148. https://doi.org/10.1016/S0955-0674(02)00314-9.

7. Yao, G., Lee, T.J., Mori, S., Nevins, J.R., and You, L. (2008). A bistable Rb-E2F switch underlies the restriction point. Nat. Cell Biol. *10*, 476–482. http://www.nature.com/ncb/journal/v10/n4/suppinfo/ncb1711_S1.html.

8. Yao, G., Tan, C., West, M., Nevins, J.R., and You, L. (2011). Origin of bistability underlying

mammalian cell cycle entry. Mol. Syst. Biol. *7*, 485. https://doi.org/10.1038/msb.2011.19.

9. Heldt, F.S., Barr, A.R., Cooper, S., Bakal, C., and Novák, B. (2018). A comprehensive model for the proliferation–quiescence decision in response to endogenous DNA damage in human cells. Proc. Natl. Acad. Sci. USA *115*, 2532–2537. https://doi.org/10.1073/pnas.1715345115.

10. Sha, W., Moore, J., Chen, K., Lassaletta, A.D., Yi, C.-S., Tyson, J.J., and Sible, J.C. (2003). Hysteresis drives cell-cycle transitions in Xenopus laevis egg extracts. Proc. Natl. Acad. Sci. USA *100*, 975–980. https://doi.org/10.1073/pnas.0235349100.

11. Pomerening, J.R., Sontag, E.D., and Ferrell, J.E., Jr. (2003). Building a cell cycle oscillator: hysteresis and bistability in the activation of Cdc2. Nat. Cell Biol. *5*, 346–351. https://doi.org/10.1038/ncb954. https://www.nature.com/articles/ncb954#supplementary-information.

12. Spencer, S.L., and Sorger, P.K. (2011). Measuring and modeling apoptosis in single cells. Cell *144*, 926–939. https://doi.org/10.1016/j.cell.2011.03.002.

13. McKenna, S., García-Gutiérrez, L., Matallanas, D., and Fey, D. (2021). BAX and SMAC regulate bistable properties of the apoptotic caspase system. Sci. Rep. *11*, 3272. https://doi.org/10.1038/s41598-021-82215-2.

14. Ballweg, R., Paek, A.L., and Zhang, T. (2017). A dynamical framework for complex fractional killing. Sci. Rep. *7*, 8002. https://doi.org/10.1038/s41598-017-07422-2.

15. Graham, T.G.W., Tabei, S.M.A., Dinner, A.R., and Rebay, I. (2010). Modeling bistable cell-fate choices in the Drosophila eye: qualitative and quantitative perspectives. Development *137*, 2265–2278. https://doi.org/10.1242/dev.044826.

16. Bednarz, M., Halliday, J.A., Herman, C., and Golding, I. (2014). Revisiting bistability in the lysis/lysogeny circuit of bacteriophage lambda. PLoS One *9*, e100876. https://doi.org/10.1371/journal.pone.0100876.

17. Jukam, D., Xie, B., Rister, J., Terrell, D., Charlton-Perkins, M., Pistillo, D., Gebelein, B., Desplan, C., and Cook, T. (2013). Opposite feedbacks in the hippo pathway for growth control and neural fate. Science *342*, 1238016. https://doi.org/10.1126/science.1238016.

18. Bouldin, C.M., Manning, A.J., Peng, Y.-H., Farr, G.H., III, Hung, K.L., Dong, A., and Kimelman, D. (2015). Wnt signaling and tbx16 form a bistable switch to commit bipotential progenitors to mesoderm. Development *142*, 2499–2507. https://doi.org/10.1242/dev.124024.

19. Schröter, C., Rué, P., Mackenzie, J.P., and Martinez Arias, A. (2015). FGF/MAPK signaling sets the switching threshold of a bistable circuit controlling cell fate decisions in embryonic stem cells. Development *142*, 4205–4216. https://doi.org/10.1242/dev.127530.

20. Fang, X., Liu, Q., Bohrer, C., Hensel, Z., Han, W., Wang, J., and Xiao, J. (2018). Cell fate potentials and switching kinetics uncovered in a classic bistable genetic switch. Nat. Commun. *9*, 2787. https://doi.org/10.1038/s41467-018-05071-1.

21. Tian, X.-J., Zhang, H., and Xing, J. (2013). Coupled reversible and irreversible bistable switches underlying TGFβ-induced epithelial to mesenchymal transition. Biophys. J. *105*, 1079–1089. https://doi.org/10.1016/j.bpj.2013.07.011.

22. Zhang, J., Tian, X.-J., Zhang, H., Teng, Y., Li, R., Bai, F., Elankumaran, S., and Xing, J. (2014). TGF-β–induced epithelial-to-mesenchymal transition proceeds through stepwise activation of multiple feedback loops. Sci. Signal. *7*, ra91. https://doi.org/10.1126/scisignal.2005304.

23. Xiong, W., and Ferrell, J.E. (2003). A positive-feedback-based bistable/'memory module/' that governs a cell fate decision. Nature *426*, 460–465.

24. Wang, L., Walker, B.L., Iannaccone, S., Bhatt, D., Kennedy, P.J., and Tse, W.T. (2009). Bistable switches control memory and plasticity in cellular differentiation. Proc. Natl. Acad. Sci. USA *106*, 6638–6643.

25. Gardner, T.S., Cantor, C.R., and Collins, J.J. (2000). Construction of a genetic toggle switch in Escherichia coli. Nature *403*, 339–342. http://www.nature.com/nature/journal/v403/n6767/suppinfo/403339a0_S1.html.

26. Kramer, B.P., and Fussenegger, M. (2005). Hysteresis in a synthetic mammalian gene network. Proc. Natl. Acad. Sci. USA *102*, 9517–9522. https://doi.org/10.1073/pnas.0500345102.

27. Xie, M., and Fussenegger, M. (2018). Designing cell function: assembly of synthetic gene circuits for cell biology applications. Nat. Rev. Mol. Cell Biol. *19*, 507–525. https://doi.org/10.1038/s41580-018-0024-z.

28. English, M.A., Gayet, R.V., and Collins, J.J. (2021). Designing biological circuits: synthetic biology within the operon model and beyond. Annu. Rev. Biochem. *90*, 221–244. https://doi.org/10.1146/annurev-biochem-013118-111914.

29. Lebar, T., Bezeljak, U., Golob, A., Jerala, M., Kadunc, L., Pirš, B., et al. (2014). A bistable genetic switch based on designable DNA-binding domains. Nat. Commun. *5*, 5007. https://doi.org/10.1038/ncomms6007.

30. Santos-Moreno, J., Tasiudi, E., Stelling, J., and Schaerli, Y. (2020). Multistable and dynamic CRISPRi-based synthetic circuits. Nat. Commun. *11*, 2746. https://doi.org/10.1038/s41467-020-16574-1.

31. Benenson, Y. (2012). Biomolecular computing systems: principles, progress and potential. Nat. Rev. Genet. *13*, 455–468. https://doi.org/10.1038/nrg3197.

32. Burrill, D.R., Inniss, M.C., Boyle, P.M., and Silver, P.A. (2012). Synthetic memory circuits for tracking human cell fate. Genes Dev. *26*, 1486–1497. https://doi.org/10.1101/gad.189035.112.

33. Ajo-Franklin, C.M., Drubin, D.A., Eskin, J.A., Gee, E.P.S., Landgraf, D., Phillips, I., and Silver, P.A. (2007). Rational design of memory in eukaryotic cells. Genes Dev. *21*, 2271–2276. https://doi.org/10.1101/gad.1586107.

34. Zhu, R., del Rio-Salgado, J.M., Garcia-Ojalvo, J., and Elowitz, M.B. (2022). Synthetic multistability in mammalian cells. Science *375*, eabg9765. https://doi.org/10.1126/science.abg9765.

35. Wu, F., Su, R.-Q., Lai, Y.-C., and Wang, X. (2017). Engineering of a synthetic quadrastable gene network to approach Waddington landscape and cell fate determination. Elife *6*, e23702. https://doi.org/10.7554/eLife.23702.

36. Tyson, J.J., Chen, K.C., and Novak, B. (2003). Sniffers, buzzers, toggles and blinkers: dynamics of regulatory and signaling pathways in the cell. Curr. Opin. Cell Biol. *15*, 221–231. https://doi.org/10.1016/S0955-0674(03)00017-6.

37. Dey, A., and Barik, D. (2021). Emergent bistable switches from the incoherent feed-forward signaling of a positive feedback loop. ACS Synth. Biol. *10*, 3117–3128. https://doi.org/10.1021/acssynbio.1c00373.

38. Song, H., Smolen, P., Av-Ron, E., Baxter, D.A., and Byrne, J.H. (2006). Bifurcation and singularity analysis of a molecular network for the induction of long-term memory. Biophys. J. *90*, 2309–2325. https://doi.org/10.1529/biophysj.105.074500.

39. Sengupta, D., and Kar, S. (2016). Unraveling the differential dynamics of developmental fate in central and peripheral nervous systems. Sci. Rep. *6*, 36397. https://doi.org/10.1038/srep36397.

40. Barra Avila, D., Melendez-Alvarez, J.R., and Tian, X.-J. (2021). Control of tissue homeostasis, tumorigenesis, and degeneration by coupled bidirectional bistable switches. PLoS Comput. Biol. *17*, e1009606. https://doi.org/10.1371/journal.pcbi.1009606.

41. Dey, A., and Barik, D. (2021). Potential landscapes, bifurcations, and robustness of tristable networks. ACS Synth. Biol. *10*, 391–401. https://doi.org/10.1021/acssynbio.0c00570.

42. Hong, T., Xing, J., Li, L., and Tyson, J.J. (2012). A simple theoretical framework for understanding heterogeneous differentiation of CD4+ T cells. BMC Syst. Biol. *6*, 66. https://doi.org/10.1186/1752-0509-6-66.

43. Zhu, J., Yamane, H., and Paul, W.E. (2010). Differentiation of effector CD4 T cell populations. Annu. Rev. Immunol. *28*, 445–489. https://doi.org/10.1146/annurev-immunol-030409-101212.

44. Antebi, Y.E., Reich-Zeliger, S., Hart, Y., Mayo, A., Eizenberg, I., Rimer, J., Putheti, P., Pe'er, D., and Friedman, N. (2013). Mapping

differentiation under mixed culture conditions reveals a tunable continuum of T cell fates. PLoS Biol. *11*, e1001616. https://doi.org/10.1371/journal.pbio.1001616.

45. Hong, T., Xing, J., Li, L., and Tyson, J.J. (2011). A mathematical model for the reciprocal differentiation of T helper 17 cells and induced regulatory T cells. PLoS Comput. Biol. *7*, e1002122. https://doi.org/10.1371/journal.pcbi.1002122.

46. Huang, B., Jolly, M.K., Lu, M., Tsarfaty, I., Ben-Jacob, E., and Onuchic, J.N. (2015). Modeling the transitions between collective and solitary migration phenotypes in cancer metastasis. Sci. Rep. *5*, 17379. https://doi.org/10.1038/srep17379.

47. Markevich, N.I., Hoek, J.B., and Kholodenko, B.N. (2004). Signaling switches and bistability arising from multisite phosphorylation in protein kinase cascades. J. Cell Biol. *164*, 353–359. https://doi.org/10.1083/jcb.200308060.

48. Li, C.-J., Liau, E.S., Lee, Y.-H., Huang, Y.-Z., Liu, Z., Willems, A., Garside, V., McGlinn, E., Chen, J.-A., and Hong, T. (2021). MicroRNA governs bistable cell differentiation and lineage segregation via a noncanonical feedback. Mol. Syst. Biol. *17*, e9945. https://doi.org/10.15252/msb.20209945.

49. Strogatz, S.H. (2000). Nonlinear Dynamics and Chaos, 1st Edition Edition (CRC Press).

50. Laslo, P., Spooner, C.J., Warmflash, A., Lancki, D.W., Lee, H.-J., Sciammas, R., Gantner, B.N., Dinner, A.R., and Singh, H. (2006). Multilineage transcriptional priming and determination of alternate hematopoietic cell fates. Cell *126*, 755–766. https://doi.org/10.1016/j.cell.2006.06.052.

51. Huang, S., Guo, Y.-P., May, G., and Enver, T. (2007). Bifurcation dynamics in lineage-commitment in bipotent progenitor cells. Dev. Biol. *305*, 695–713. https://doi.org/10.1016/j.ydbio.2007.02.036.

52. Guantes, R., and Poyatos, J.F. (2008). Multistable decision switches for flexible control of epigenetic differentiation. PLoS Comput. Biol. *4*, e1000235. https://doi.org/10.1371/journal.pcbi.1000235.

53. Wang, J., Zhang, K., Xu, L., and Wang, E. (2011). Quantifying the Waddington landscape and biological paths for development and differentiation. Proc. Natl. Acad. Sci. USA. *108*, 8257–8262. https://doi.org/10.1073/pnas.1017017108.

54. Ferrell, J.E. (2012). Bistability, bifurcations, and Waddington's epigenetic landscape. Curr. Biol. *22*, R458–R466. https://doi.org/10.1016/j.cub.2012.03.045.

STAR★METHODS

KEY RESOURCES TABLE

REAGENT or RESOURCE	SOURCE	IDENTIFIER
Software and algorithms		
MATLAB R2016b	MathWorks (Natick, MA)	https://www.mathworks.com/products/matlab.html
MATLAB code for simulation	This work	https://github.com/dbarikUoH/NonCanonical-BS-Switches.git

RESOURCE AVAILABILITY

Lead contact

Further information and requests for resources should be directed to and will be fulfilled by the lead contact Debashis Barik (dbariksc@uohyd.ac.in)

Materials availability

This study did not generate new materials or reagents.

Data and code availability

Data reported in this paper will be shared by the lead contact upon request. All original code has been deposited at Github and is publicly available as of the date of publication. DOIs are listed in the key resources table. Any additional information required to reanalyze the data reported in this paper is available from the lead contact upon request.

METHOD DETAILS

Mathematical models of the networks

To investigate these noncanonical switches, we modeled the networks using nonlinear ordinary differential equations. As ultrasensitivity in activation/deactivation of the target gene is a key ingredient to bistability, we used Hill function to model the ultrasensitive activation/deactivation of a target gene. In general, the activation of a target gene (X) by another gene (Y) is expressed by the Hill function as

$$H^{+}_{XY}(Y) = \frac{\left(Y/J_{XY}\right)^{n_{XY}}}{1+\left(Y/J_{XY}\right)^{n_{XY}}} \quad \text{(Equation 1)}$$

where n_{XY} and J_{XY} are the Hill coefficient and activation threshold, respectively. The inhibition of the gene is represented by $H^{-}_{XY} = 1 - H^{+}_{XY}$. When a target gene is regulated by multiple regulatory signals, the functionality of the gene may need to satisfy logic gate configurations. To address this, we have investigated both the OR- and AND-gate configurations of the gene A and B in the networks. In the OR-gate, the net regulatory influence on a target gene is represented by the summation of the individual inputs. As a representative case, the dynamical equations for the ppMI network are given as

$$\frac{dA}{dt} = g_{A0} + g_{AS}H^{+}_{AS}(S) + g_{AB}H^{-}_{AB}(B) - \gamma_A A \quad \text{(Equation 2)}$$

$$\frac{dB}{dt} = g_{B0} + g_{BS}H^{+}_{BS}(S) + g_{BA}H^{-}_{BA}(A) - \gamma_B B \quad \text{(Equation 3)}$$

g_{X0}, g_{XY} and γ_X represent the unregulated synthesis, maximal synthesis and degradation rates of X. On the contrary, the net regulatory influence on a target gene is represented by the multiplication of the individual inputs in the AND-gate configuration. The dynamical equations for the same network are given as

$$\frac{dA}{dt} = g_{A0} + g_{A1}H^{+}_{AS}(S)H^{-}_{AB}(B) - \gamma_A A \quad \text{(Equation 4)}$$

$$\frac{dB}{dt} = g_{B0} + g_{B1} H^{+}_{BS}(S) H^{-}_{BA}(A) - \gamma_B B \quad \text{(Equation 5)}$$

The dynamical equations for all networks are listed in the Table S2.

Bifurcation analysis using pseudo-potential energy

1-p bifurcation analysis is required to determine the nature of the bistability and more importantly, such analysis must be carried out for every network under random variation of parameters to determine the topological and parametric requirements of noncanonical bistability. We have used our recently developed pseudo potential energy based bifurcation analysis method to carry out high-throughput bifurcation analysis with automated parameter searching for various types of bistable switches.[37,41] The principle of generating a bifurcation diagram from the pseudo potential energy is that the steady states of the dynamical systems are reflected as the extrema in the potential energy landscape.[53,54] The stable and unstable steady states of the nonlinear dynamical systems must be manifested as the minima and maxima, respectively. Thus, in principle a bifurcation diagram can be generated by retrieving the qualitative nature and quantitative value of the steady states from the extrema in the potential landscape. However, the lack of a general definition of potential energy in multidimensional dynamical systems poses a challenge in the calculation of potential energy.[53] We overcome this problem by reducing the two-dimensional systems of the networks into a one-dimensional representation by applying transfer function method. Specifically, one of the variables was expressed in terms of the other variable at steady state and substituted it in the equation of the other variable to obtain an effective potential energy in one dimension.[37,41] Such dimensional reduction is justified as the bifurcation analysis itself is the determination of fixed points where the system is time independent.[49] As an example, in the ppMI network under OR-gate, A was expressed in terms of B at steady state as (from Equation 2)

$$A = \mathcal{G}(S, B) \quad \text{(Equation 6)}$$

where $\mathcal{G}(S, B) = (g_{A0} + g_{AS} H^{+}_{AS}(S) + g_{AB} H^{-}_{AB}(B))/\gamma_A$. Substituting A in the equation of B results a one-dimensional description of the system as

$$\frac{dB}{dt} = g_{B0} + g_{BS} H^{+}_{BS}(S) + g_{BA} H^{-}_{BA}(\mathcal{G}(S, B)) - \gamma_B B \quad \text{(Equation 7)}$$

where the expression on the right-hand side represents the effective force. The effective pseudo potential energy of the system can be obtained by integrating the force as

$$V(S, B) = -\int_0^B \left[g_{B0} + g_{BS} H^{+}_{BS}(S) + g_{BA} H^{-}_{BA}(\mathcal{G}(S, x)) - \gamma_B x \right] dx \quad \text{(Equation 8)}$$

The effective potential energy, $V(S,B)$, dictates the steady state properties of the system. To determine the 1-p bifurcation diagram from the pseudo-potential energy (Equation 8), we calculated the pseudo-potential energy as a function of the B at each S using the cumulative trapezoidal method of numerical integration in MATLAB. We evaluated the local extrema in the potential function using the *findpeaks* function and determined the values of the steady states from the locations (B coordinate) of the extrema. The steady state associated with the minima and the maxima in the potential energy are classified as stable and unstable steady states, respectively. Thus, at each S we determined both quantitative and qualitative information about the steady states from the potential energy function. We repeated this procedure to determine the quantitative and qualitative change in the steady states with variation of the bifurcation parameter, S, and thus constructing a full 1-p bifurcation diagram. At the SN bifurcation point a pair of stable and unstable steady states is born (or destroyed), and thus monitoring of the creation and annihilation of a minimum and maximum adjacent to each other allowed us to determine the SN point. See Figures S9–S14 for overlaid plots of 1-p bifurcation diagrams along with the contours of pseudo potential energy $V(S, B)$ for various types of bistable switches. In these supporting figures we also plotted the $V(S, B)$ as a function of B to highlight the appearance and disappearance of local minima with the change in the bifurcation parameter, S.

Identification of various types of bistable switches

During the bifurcation calculation, we identified the type of bistable switch by exploiting the number of SN bifurcation points (N), number of jumps in the stable steady state values at the bifurcation points (J) and the direction of jump (Table S3). It is apparent that different types of bistable switches cannot be distinguished only based on the number of SN points and thus additional signatory feature is needed to identify the switches during the bifurcation calculations. Therefore, we devised a method to determine the jump

pattern of the stable branch at the bifurcation points. In the same array we stored the values of the steady state of the monostable region and the lower stable steady state of the bistable region. The upper stable steady state of the bistable region was stored in a separate array. The value of the stable steady state, stored in the first array, changes sharply at the bifurcation point creating a signatory pattern of jumps depending of the type of the bistable switch. For example, both the forward and backward facing Bs switches contain two SN points (N = 2) and thus they are distinguished from one another from the different direction of jump (J = 1) of the stable branch. Is and InIs switches both consist of two SN points (N = 2), however the first array of stable steady states does not exhibit any sharp change at the bifurcation point (J = 0) for the Is switch. On the contrary there are two jumps (J = 2) for InIs switch. The number of SN points, jumps and their directions are listed in the Table S3.

Parameter search for bistable switches

We implemented an automated parameter searching procedure to find a parameter set for bistable switches. In this procedure 1-p bifurcation analysis was performed for randomly chosen parameter combinations. All parameters, except the activation/inhibition thresholds (J_{XY}) were sampled from independent uniform distributions having a particular range (See Table S4). The ranges are selected in such a way that the expression level falls in the biologically relevant range. In order to avoid bias in the threshold values, we adopted the half-functional rule to ensure that the randomly chosen threshold values are not biased towards either activation or inhibition.[37] The sample space for parameter combination was 900,000 and thus a total of 900,000 1-p bifurcation analyses were performed for every network. During the bifurcation calculation, type of the bistable switches were also determined based on J, N and jump pattern in the value of the stable steady state at the bifurcation points. We counted the number of various types of switches that each network produced and determined the occurrence probability of the switches.

Phase diagrams of bistable switches

We calculated phase diagrams of noncanonical switches by running 1-p bifurcation analysis with respect to the bifurcation parameter S repeatedly for a range of values of two other parameters keeping remaining parameters unchanged. In each combination of these two parameters, we determined the type of bistable switch generated. By repeating this procedure for a range of values of these two parameters, we created a two-dimensional lattice consisting of information about the identity of the bistable switch represented by a particular color in the phase diagram. Depending on the range of parameter values the step length for the two secondary parameters were either 0.25 or 0.5 and to construct a phase diagram ~30000-113750 1-p bifurcations calculations were performed. The phase diagram calculations considered a possibility of 126 unique bistable switches that may originate from the fusion of Bs, Is and Msh as basic building blocks (See Table S7).

2-p bifurcation analysis

We repeated 1-p bifurcation analysis with respect to the signal S for different values of a secondary parameter and recorded the locations of two SN bifurcation points. Furthermore, during this calculation the identity of the bistable switch was also determined. We plotted the locus of the two SN bifurcation points as a function of the secondary parameter to construct the 2-p bifurcation plots color coded based on the type of bistable switch.

QUANTIFICATION AND STATISTICAL ANALYSIS

The total counts of various types of bistable switches were quantified in the high-throughput (900,000 runs) 1-p bifurcation runs of each network.

ADDITIONAL RESOURCES

None.